PHYSICAL REVIEW A **68**, 052308 (2003)

Teleportation of continuous-variable polarization states

A. Dolińska,[1] B. C. Buchler,[1] W. P. Bowen,[1] T. C. Ralph,[2] and P. K. Lam[1]
[1]*Quantum Optics Group, Department of Physics, Faculty of Science, Australian National University, Australian Capital Territory 0200, Australia*
[2]*Department of Physics, University of Queensland, Queensland 4072, Australia*
(Received 10 July 2003; published 6 November 2003)

This paper discusses methods for the optical teleportation of continuous-variable polarization states. We show that using two pairs of entangled beams, generated using four squeezed beams, perfect teleportation of optical polarization states can be performed. Restricting ourselves to three squeezed beams, we demonstrate that polarization state teleportation can still exceed the classical limit. The three-squeezer schemes involve either the use of quantum nondemolition measurement or biased entanglement generated from a single squeezed beam. We analyze the efficacies of these schemes in terms of fidelity, signal transfer coefficients, and quantum correlations.

DOI: 10.1103/PhysRevA.68.052308 PACS number(s): 03.67.Hk, 42.50.Dv, 42.65.Yj

I. INTRODUCTION

Quantum teleportation [1] is an important operation for the transmission and manipulation of quantum states and information. It has been experimentally demonstrated in both discrete [2] and continuous-variable [3,4] regimes. To date, continuous-variable teleportation protocols have been performed solely on the quadrature amplitudes of optical fields. Recently there has been growing interest in continuous-variable polarization states in the context of quantum information schemes. Experimental demonstrations of polarization squeezing [5–9] and entanglement [10] have been performed. A practical advantage of polarization states when applied to quantum information networks is that a network-wide frequency reference is not required [11]. Furthermore, quantum communication networks are expected to require the ability to transfer quantum information between optical and atomic states. This has been experimentally demonstrated between optical polarization states and atomic spin ensembles [8]. It is then natural to ask how quantum teleportation can be optimally implemented on continuous-variable polarization states.

This paper is arranged in the following way. Section II reviews the use of Stokes operators to characterize the quantum properties of polarized light. In Sec. III we discuss two commonly used teleportation figures of merit in the context of quadrature teleportation. Section IV proposes a straightforward generalization of quadrature teleportation to polarization teleportation, and generalizes the teleportation figures of merit to polarization states. In Secs. V, VI, and VII modifications of this protocol, which optimize these figures of merit are discussed. We summarize and conclude in Sec. VIII.

II. BACKGROUND

In classical optics the polarization state of light can be described using Stokes parameters, where an arbitrary polarization state is decomposed into three components: linear (vertical/horizontal), diagonal ($+45°/-45°$), and circular (left/right handed) [12]. This vector representation can be elegantly visualized on a Poincaré sphere shown in Fig. 1. The orientation of the Stokes vector describes the polarization state of the laser beam with $\hat{S}_1$ giving the intensity difference between the horizontally and vertically polarized components of the beam and $\hat{S}_2$ giving the intensity difference between the diagonally and antidiagonally polarized components. The azimuthal deviation from the $\hat{S}_1$-$\hat{S}_2$ plane towards the $\hat{S}_3$ axis indicates the ellipticity of the polarization state. By drawing an analogy with classical Stokes parameters a set of Stokes operators can be defined, providing a convenient description of the quantum polarization properties of light [13,14]:

$$\begin{aligned}\hat{S}_0&=\hat{a}_H^\dagger\hat{a}_H+\hat{a}_V^\dagger\hat{a}_V=\hat{n}_H+\hat{n}_V,\\ \hat{S}_1&=\hat{a}_H^\dagger\hat{a}_H-\hat{a}_V^\dagger\hat{a}_V=\hat{n}_H-\hat{n}_V,\\ \hat{S}_2&=\hat{a}_H^\dagger\hat{a}_V e^{i\theta}+\hat{a}_V^\dagger\hat{a}_H e^{-i\theta}=\hat{n}_D-\hat{n}_{\bar{D}},\\ \hat{S}_3&=i\hat{a}_V^\dagger\hat{a}_H e^{-i\theta}-i\hat{a}_H^\dagger\hat{a}_V e^{i\theta}=\hat{n}_R-\hat{n}_L.\end{aligned} \tag{1}$$

Here the polarization mode is constructed in terms of annihilation $\hat{a}$ and creation $\hat{a}^\dagger$ operators of the horizontal H and vertical V constituent modes, with a phase θ between them. These operators can be written as $\hat{a}(t)=\alpha+\delta\hat{a}(t)$, where α is the classical amplitude and $\delta\hat{a}(t)$ is the operator containing the quantum fluctuations with $[\delta\hat{a}(t),\delta\hat{a}^\dagger(t)]=1$ and $\langle\delta\hat{a}(t)\rangle=0$. We will assume that $|\alpha|=\langle|\hat{a}(t)|\rangle \gg\langle|\delta\hat{a}(t)|^2\rangle$, allowing a linearization of the operator equations.

$\hat{S}_0$ commutes with the other Stokes operators and its expectation value is proportional to the total intensity of the light beam. $\hat{S}_1$, $\hat{S}_2$, and $\hat{S}_3$, however, obey a coupled set of commutation relations and are isomorphic to the Pauli matrices: $[\hat{S}_l,\hat{S}_m]=2i\hat{S}_n$, where $\{l,m,n\}=\{1,2,3\}$ and are cyclically interchangeable. This says that simultaneous measurements of these Stokes operators are, in general, impossible and their variances are restricted by

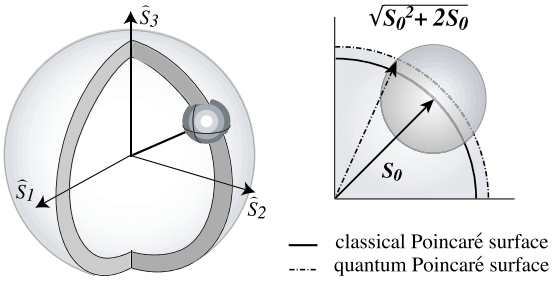

FIG. 1. The quantum Poincaré sphere. In the classical case S_0, the total photon number is the radius of the sphere, whereas in quantum picture the radius takes a larger value of $\sqrt{S_0^2+2S_0}$ due to the quantum uncertainty [11]. The presence of the uncertainty relations [Eq. (2)] manifests itself in the quantum noise "ball" as indicated.

$$V_l V_m \geqslant |\langle \hat{S}_n \rangle|^2. \tag{2}$$

Here, $V_l = \langle (\hat{S}_l)^2 \rangle - \langle \hat{S}_l \rangle^2$ is the variance of each Stokes operator.

The length of the quantum Stokes vector in Fig. 1 is $\sqrt{\langle S_0^2 \rangle + 2\langle S_0 \rangle}$, which always exceeds its classical counterpart. The coupled uncertainty relations of the Stokes variances in Eq. (2) are exhibited further in the appearance of a three-dimensional noise "ball," superimposed on the Poincaré surface, at the end of the Stokes vector. In the case of coherent polarization states this ball is spherical.

The field operators $\hat{a}(t), \hat{a}^\dagger(t)$ are now expanded in terms of their dc and fluctuating components. Keeping only the first-order fluctuation terms, Eqs. (1) yield linearized equations for the fluctuations in the Stokes operators:

$$\delta\hat{S}_0 = \alpha_H \delta X_H^+ + \alpha_V \delta X_V^+ , \tag{3}$$

$$\delta\hat{S}_1 = \alpha_H \delta X_H^+ - \alpha_V \delta X_V^+ , \tag{4}$$

$$\delta\hat{S}_2 = \alpha_H (\delta X_V^- \sin\theta + \delta X_V^+ \cos\theta) + \alpha_V (\delta X_H^+ \cos\theta - \delta X_H^- \sin\theta), \tag{5}$$

$$\delta\hat{S}_3 = \alpha_H (\delta X_V^+ \sin\theta - \delta X_V^- \cos\theta) + \alpha_V (\delta X_H^- \cos\theta + \delta X_H^+ \sin\theta), \tag{6}$$

where $\hat{X}^{+(-)}$ are the usual amplitude (phase) quadrature operators, defined as $\delta\hat{X}^+ = (\delta\hat{a} + \delta\hat{a}^\dagger)$ and $\delta\hat{X}^- = i(\delta\hat{a}^\dagger - \delta\hat{a})$. It can be seen from Eqs. (4)–(6) that the linearized Stokes operators are a linear combination of the quadrature operators for the two modes.

In this paper we are interested in fluctuations at a frequency ω around the optical carrier frequency. The Fourier transform of the time domain Stokes operators will be taken from now on, with all the operators being in the frequency domain. We include the signal at frequency ω, encoded on polarization modulation as a classical fluctuations term, making $\hat{a} = \alpha_c + \delta\hat{a}_q + \delta a_c$. Unlike quantum fluctuations $\delta\hat{a}_q$, the introduced δa_c term is purely classical with $[\delta a_c, \delta a_c^\dagger] = 0$. The $\hat{a}$ operator expansions substituted into Stokes equations (1) yield linearized Eqs. (4)–(6) in frequency domain where $\delta\hat{X}^\pm = \delta X_c^\pm + \delta\hat{X}_q^\pm$. Hence there are two independent sources of fluctuations, the classical signal c and the quantum noise q. The variances $V(\delta\hat{S}_l)$ of the Stokes operators may be calculated from Eqs. (4)–(6):

$$V_{S_1} = \alpha_H^2 (V_{H,c}^+ + V_{H,q}^+) + \alpha_V^2 (V_{V,c}^+ + V_{V,q}^+) + 2\alpha_H \alpha_V \langle \delta X_{V,c}^+ \delta X_{H,c}^+ \rangle, \tag{7}$$

$$V_{S_2} = \alpha_H^2 (\cos\theta)^2 (V_{V,c}^+ + V_{V,q}^+) + \alpha_V^2 (\cos\theta)^2 (V_{H,c}^+ + V_{H,q}^+) + \alpha_H^2 (\sin\theta)^2 (V_{V,c}^- + V_{V,q}^-) + \alpha_V^2 (\sin\theta)^2 (V_{H,c}^- + V_{H,q}^-)$$
$$+ 2\alpha_H \alpha_V \sin\theta \cos\theta \langle \delta X_{V,c}^- \delta X_{H,c}^+ \rangle + 2\alpha_H \alpha_V (\cos\theta)^2 \langle \delta X_{V,c}^+ \delta X_{H,c}^+ \rangle + 2\alpha_H^2 \sin\theta \cos\theta \langle \delta X_{V,c}^+ \delta X_{V,c}^- \rangle$$
$$- 2\alpha_H \alpha_V \sin\theta \cos\theta \langle \delta X_{V,c}^+ \delta X_{H,c}^- \rangle - 2\alpha_H \alpha_V (\sin\theta)^2 \langle \delta X_{V,c}^- \delta X_{H,c}^- \rangle - 2\alpha_V^2 \sin\theta \cos\theta \langle \delta X_{H,c}^+ \delta X_{H,c}^- \rangle, \tag{8}$$

$$V_{S_3} = \alpha_H^2 (\cos\theta)^2 (V_{V,c}^- + V_{V,q}^-) + \alpha_V^2 (\cos\theta)^2 (V_{H,c}^- + V_{H,q}^-) + \alpha_H^2 (\sin\theta)^2 (V_{V,c}^+ + V_{V,q}^+) + \alpha_V^2 (\sin\theta)^2 (V_{H,c}^+ + V_{H,q}^+)$$
$$+ 2\alpha_H \alpha_V \sin\theta \cos\theta \langle \delta X_{V,c}^+ \delta X_{H,c}^- \rangle + 2\alpha_H \alpha_V (\sin\theta)^2 \langle \delta X_{V,c}^+ \delta X_{H,c}^+ \rangle + 2\alpha_V^2 \sin\theta \cos\theta \langle \delta X_{H,c}^+ \delta X_{H,c}^- \rangle$$
$$- 2\alpha_H \alpha_V \sin\theta \cos\theta \langle \delta X_{V,c}^- \delta X_{H,c}^+ \rangle - 2\alpha_H \alpha_V (\cos\theta)^2 \langle \delta X_{V,c}^- \delta X_{H,c}^- \rangle - 2\alpha_H^2 \sin\theta \cos\theta \langle \delta X_{V,c}^+ \delta X_{H,c}^- \rangle. \tag{9}$$

The variance terms with subscript "c" represent a delierately applied signal, distinct from the quantum noise terms with subscript "q." In general, classical modulation correlations can exist and additional cross terms, such as $\langle \delta X_{H,c}^+ \delta X_{V,c}^+ \rangle$, may appear. These are included for completeness, although they are not considered in the modeling that follows in later sections. In the following sections, we will assume that the light beams are pure states with Gaussian statistics. Unless squeezed, the quantum terms will be at the standard quantum limit and $V_{H/V,q}^\pm = 1$.

III. FIGURES OF MERIT FOR QUADRATURE TELEPORTATION

The figures of merit that we consider here for polarization teleportation are generalizations of those previously used for

quadrature teleportation, namely, the T-V measure and fidelity [4]. In this section, we present the relevant definitions of quadrature teleportation. The extension of the parameters is then presented in later sections.

Fidelity is one way to quantify the success of a quantum state reconstruction for many quantum protocols. It is given by the overlap integral of the initial and final wave functions, $\mathcal{F}=|\langle\psi_{\rm in}|\hat{\rho}_{\rm out}|\psi_{\rm in}\rangle|^2$, where $|\psi_{\rm in}\rangle$ is the input state and $\hat{\rho}_{\rm out}$ is the density operator of the output. For Gaussian input states the statistics of a laser beam are fully described by the first two statistical moments: the mean and the variance. When unity gain is assumed for the reconstruction, that is, the output state has the same classical amplitude as the input, and when the input states are coherent, i.e., $V_{\rm in}^{\pm}=1$, the expression for fidelity is given by

$$\mathcal{F}=\frac{2}{\sqrt{(V_{\rm out}^{+}+1)(V_{\rm out}^{-}+1)}}, \tag{10}$$

where $V_{\rm out}^{\pm}$ are the output quadrature variances. Variations away from unity gain typically lead to an exponentially decreasing fidelity value [4].

The case of $\mathcal{F}=0$ implies that the input and the output are orthogonal and bear no resemblance to each other, while $\mathcal{F}=1$ suggests perfect reconstruction of the input. In the absence of entanglement, the classical fidelity limit for the quadrature teleportation of a coherent state is $\mathcal{F}\leqslant\frac{1}{2}$ [3].

Another useful way of quantifying teleportation is via a T-V diagram [16]. Here two parameters are considered. The first parameter is the signal transfer coefficient $T^{\pm}$, which is the ratio of the signal-to-noise ratio $\mathcal{R}$ of the output to that of the input for a given quadrature,

$$T_q=T^{+}+T^{-}=\frac{\mathcal{R}_{\rm out}^{+}}{\mathcal{R}_{\rm in}^{+}}+\frac{\mathcal{R}_{\rm out}^{-}}{\mathcal{R}_{\rm in}^{-}}. \tag{11}$$

When no information is recovered there is no signal, hence $T_q=0$. For ideal teleportation, the transfer coefficient has $\mathcal{R}_{\rm in}^{\pm}=\mathcal{R}_{\rm out}^{\pm}$ for both quadratures, as the vacuum noise problem is circumvented. This gives the ideal two quadrature limit of $T_q^{\rm max}=2$. The classical limit at unity gain is given by $T_q^{\rm classical}=\frac{2}{3}$.

The second parameter of the T-V diagram is the conditional variance, $V_{\rm cv}=\frac{1}{2}(V_{\rm cv}^{+}+V_{\rm cv}^{-})$, which is a measure of the correlation between the input and the output quadratures, and is defined as

$$V_{\rm cv}^{\pm}=V_{\rm out}^{\pm}-\frac{\langle|\delta\hat{X}_{\rm in}^{\pm}\delta\hat{X}_{\rm out}^{\pm}|^2\rangle}{V_{\rm in}^{\pm}}. \tag{12}$$

For Gaussian input states, it can be shown that $V_{\rm cv}^{\pm}=V_{\rm out}^{\pm}(1-T^{\pm})$, where $V_{\rm out}$ is the output of the system with no signal input [16]. The conditional variance is a measure of quantum correlation between the input and the output states and it reflects the amount of noise added to the output state by the teleporter. Ideal quadrature teleportation replicates the input exactly, giving the lower bound of $V_{\rm cv}^{\rm min}=0$. At unity gain the classical limit is again the double vacuum noise penalty. Hence $V_{\rm cv}^{\rm classic}=2$.

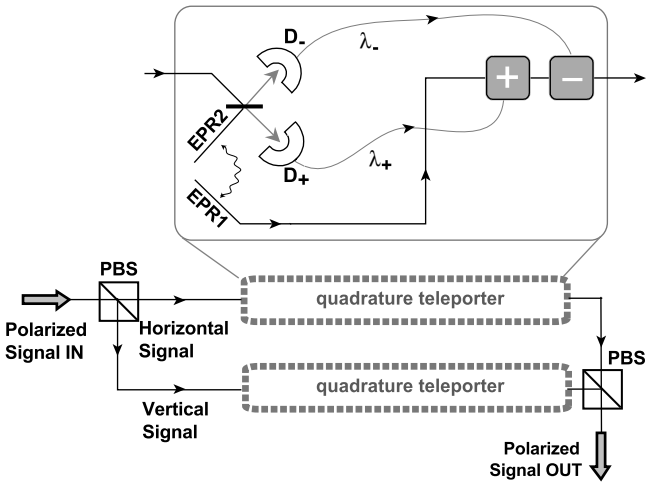

FIG. 2. Polarization state teleportation scheme with twin teleporters. EPR1,2, two entangled beams; $D_{\pm}$, amplitude/phase homodyne detectors; $+/-$, amplitude/phase modulators; $\lambda_{\pm}$, amplitude/phase feed-forward gains; and PBS, polarizing beamsplitter. A standard quadrature teleporter is shown in the inset.

The T_q and $V_{\rm cv}$ parameters can be plotted on a T-V diagram as a function of the teleportation feed-forward gains. Once evaluated, both Eqs. (11) and (12) become independent of the input signal amplitudes and Eq. (12) is also independent of the input noise.

Note that a more stringent teleportation criteria is the passing of the no-cloning limit [17]. At unity gain this corresponds to a fidelity of 2/3 or equivalently to entering the lower right-hand quadrant of the T-V diagram. For simplicity we consider here only the two criteria described above.

IV. POLARIZATION STATE TELEPORTATION WITH TWIN TELEPORTERS

We note from Eqs. (7)–(9) that polarization states can be completely described by the quadrature amplitudes of both the horizontal and vertical polarization modes. The obvious way to teleport an input polarization state is, therefore, to decompose the input beam into a horizontally and a vertically polarized beam via a polarizing beam splitter as shown in Fig. 2 [18]. Two standard continuous-variable quadrature amplitude teleporters, one for each polarization mode, can be used to teleport the orthogonally polarized beams The complete task thus requires four squeezed beams for the generation of two pairs of quadrature entanglement. Finally, the teleported states are recombined at the receiving station using another polarizing beamsplitter.

The teleportation fidelity for this system is shown in Fig. 7(a). Assuming that all four beams are equally squeezed, the expression for the fidelity of the twin teleporters scheme becomes

$$\mathcal{F}=\frac{1}{(V_{\rm SQ}+1)^2}, \tag{13}$$

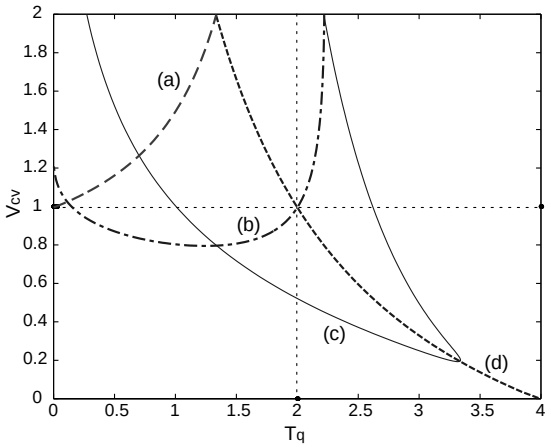

FIG. 3. *T*-*V* plot of the teleportation of polarization state with twin teleporters (a) with coherent states, (b) with 3-dB squeezing ($V_{SQ}=0.5$), and (c) with 10-dB squeezing ($V_{SQ}=0.1$) as a function of feed-forward gain. (d) Locus of unity gain points from no squeezing to perfect squeezing.

where V_{SQ} is the variance of the squeezed quadratures of the beams used to produce the entanglement. Since the fidelities for the vertical and horizontal modes are independent, the fidelity is calculated from a four-dimensional overlap integral between the input and output states. Equation (13) is derived simply by squaring the quadrature teleporter fidelity. We note that the classical limit of this polarization teleporter is $\mathcal{F}\leqslant\frac{1}{4}$ and ideal polarization teleportation has fidelity 1.

The results of *T*-*V* analysis for this scheme are illustrated in Fig. 3. Similar to the quadrature teleporter, the conditional variance is now extended to $V_{cv}=\frac{1}{4}(V^{+}_{cv,H}+V^{-}_{cv,H}+V^{+}_{cv,V}+V^{-}_{cv,V})$ and the total signal transfer coefficient is now given by $T_q=T^{+}_{H}+T^{-}_{H}+T^{+}_{V}+T^{-}_{V}$. For ideal squeezing, we obtain $V_{cv}\rightarrow 0$ and $T_q\rightarrow 4$.

So far, we have chosen to ignore the classical amplitude of our input state. Although the fluctuations in the input polarization are teleported by the twin teleporters, the polarization of the input carrier field is not teleported. This is, at first thought, analogous to quadrature teleportation where the carrier amplitude, or the optical intensity, of the input beam is assumed to be unimportant in the reconstruction of the quantum state at the sideband frequency. Besides, it is relatively trivial to replicate the input intensity at the output. Interestingly, however, Eqs. (7)–(9) suggest that the polarization of the input carrier field cannot be ignored in the teleportation of polarization states. This is due to the fact that uncertainty relations of Stokes operators are directly scaled by the carrier polarization. The carrier field polarization consists of two amplitudes (the horizontal and vertical components) as well as one relative phase angle. Polarization fluctuations will only be teleported properly provided the input polarization is known and the output polarization is set to be identical. A complete polarization teleporter would therefore include the twin teleporters plus an optical setup presented in Fig. 4 to shift an arbitrary carrier field polarization to a set polarization and then, after the teleportation protocol, return it to its original polarization.

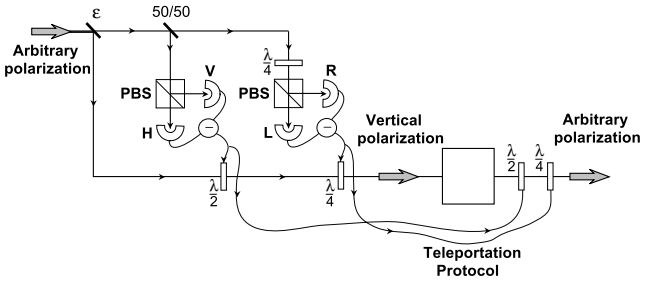

FIG. 4. Classical control system for measuring and controlling the polarization of carrier field. This figure demonstrates that input polarization state can be measured and fed forward to control the polarization state of another beam. ε, beam splitter with low transmittivity; H/V, horizontal/vertical polarization detection; R/L, right/left circular polarization detection; PBS, polarizing beam splitter; $\lambda/2$, half-wave plate; and $\lambda/4$, quarter-wave plate. The vertical output is subsequently teleported by a chosen protocol and returned back to its original polarization at the receiving station.

V. SQD-TELEPORTER SCHEME

Inspection of the Stokes operators shows that since $\hat{S}_0$ commutes with $\hat{S}_1$, $\hat{S}_2$, and $\hat{S}_3$, it can be measured with no penalty on the remaining three operators. For quadrature teleportation two squeezed beams enable teleportation of two variables $\delta\hat{X}^{-}$ and $\delta\hat{X}^{+}$. This raises the question of whether polarization teleportation could be achieved using only three squeezed beams (for $\hat{S}_1$, $\hat{S}_2$, and $\hat{S}_3$) rather than the four utilized in the previous scheme.[1] Choosing the polarization of the carrier beam to be vertical causes the α_H terms in Eqs. (4)–(6) to vanish, giving

$$\delta\hat{S}_1^{\mathrm{SQD}}=-\alpha_V\delta X_V^{+}, \tag{14}$$

$$\delta\hat{S}_2^{\mathrm{SQD}}=\alpha_V(\delta X_H^{+}\cos\theta-\delta X_H^{-}\sin\theta), \tag{15}$$

$$\delta\hat{S}_3^{\mathrm{SQD}}=\alpha_V(\delta X_H^{-}\cos\theta+\delta X_H^{+}\sin\theta). \tag{16}$$

The linearized variances for the vertical carrier Stokes fluctuations from Eqs. (7)–(9) now simplify to

$$V^{\mathrm{SQD}}_{\delta\hat{S}_1}=\alpha_V^2V_V^{+}, \tag{17}$$

$$V^{\mathrm{SQD}}_{\delta\hat{S}_2}=\alpha_V^2(\cos\theta)^2V_H^{+}+\alpha_V^2(\sin\theta)^2V_H^{-}-2\alpha_V^2\sin\theta\cos\theta\langle\delta X^{+}_{H,c}\delta X^{-}_{H,c}\rangle, \tag{18}$$

$$V^{\mathrm{SQD}}_{\delta\hat{S}_3}=\alpha_V^2(\cos\theta)^2V_H^{-}+\alpha_V^2(\sin\theta)^2V_H^{+}+2\alpha_V^2\sin\theta\cos\theta\langle\delta X^{+}_{H,c}\delta X^{-}_{H,c}\rangle, \tag{19}$$

where the variances $V^{\pm}_{H/V}=V^{\pm}_{c}+V^{\pm}_{q}$ are the sum of classical signal and quantum fluctuation variances. The classical cross

[1]This can be done without loss of generality so long as the setup in Fig. 4 is utilized.

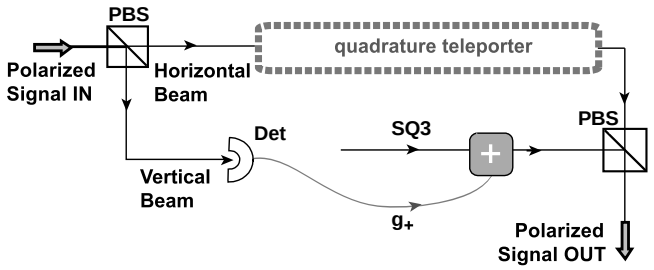

FIG. 5. SQD-teleporter experimental setup consisting of a direct detection SQD measurement and a quadrature teleporter circuit. Det, standard amplitude detector; +, amplitude modulator, g_+, amplitude modulator gain, and PBS, polarizing beam splitter.

correlation terms in Eqs. (7)–(9) have now reduced so that only correlations between the phase and amplitude quadratures of the horizontal input mode remain.

The phase angle θ has no effect on the classical polarization since $\alpha_H=0$, therefore making the angle between α_V and α_H meaningless. It does nevertheless appear in the expressions for the variances of the Stokes operators, although the angle is not referenced to a carrier field. The situation is analogous to the case of a squeezed vacuum state where its quadrature angle, although lacking reference to a carrier amplitude, affects the variance.

The uncertainty relations in Eq. (2) are strongly affected by choosing $\langle\hat{a}_H\rangle=0$ since this also implies $\langle\hat{S}_2\rangle=\langle\hat{S}_3\rangle=0$. From Eq. (2), the only uncertainty remaining is that between $\hat{S}_2$ and $\hat{S}_3$. Quantum teleportation of these two quantities can be achieved via a single entangled pair. $\hat{S}_1$ on the other hand commutes with $\hat{S}_2$ and $\hat{S}_3$ and can be determined without disturbing them, therefore its reconstruction does not require a second entangled pair. In other words, Eqs. (15) and (16) are seen to completely decouple from Eq. (14). The vertical amplitude fluctuations of $\delta\hat{S}_1^{\mathrm{SQD}}$ can therefore be reproduced by a single quadrature (SQD) measurement [19].

The schematic of this SQD protocol is shown in Fig. 5. Vertically polarized light is incident at the input polarizing beam splitter. The bright vertical light mode is reflected and detected. The resulting photocurrent is used to control the amplitude modulation of a vertically polarized squeezed beam SQ3. The amplitude quadrature of the modulated beam SQ3 will, in the limit of ideal squeezing and appropriate feed-forward gain, be identical to $\delta\hat{X}_V^+$, the amplitude quadrature of the vertically polarized light at the input to the teleporter. Since $\delta\hat{S}_1^{\mathrm{SQD}}\propto\delta\hat{X}_V^+$ this single quadrature feed-forward loop is enough to teleport $\delta\hat{S}_1$. The quadrature teleportation protocol, using an EPR pair, transfers the fluctuations of $\delta\hat{S}_2^{\mathrm{SQD}}$ and $\delta\hat{S}_3^{\mathrm{SQD}}$ onto the horizontally polarized output beam EPR1 [16]. The vertical and horizontal output modes are then combined via a second polarizing beam splitter and the polarization information is recreated. It is important to ensure that the horizontal output mode (EPR1) has much less power than the vertical output beam SQ3, in order to preserve the input polarization.

The above scheme is not necessarily limited only to vertically polarized input states. An arbitrary input state can be rotated using a variable half- and quarter-wave plate arrangement and feedback loops, such as that in Fig. 4, to ensure all of the light power is in the SQD part of the system and its polarization is vertical. Once the protocol is complete, it can be rotated back to its original polarization.

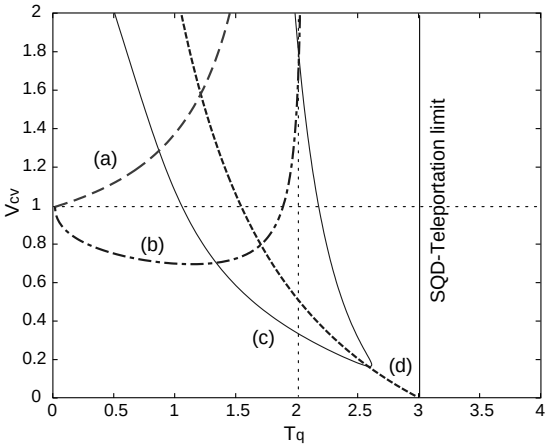

FIG. 6. The SQD-teleporter T-V plot using only three quadratures of interest, with $V_{SQ3}=V_{SQ}$. (a) With coherent states. (b) With 3-dB squeezing ($V_{\mathrm{SQ}}=0.5$), and (c) with 10-dB squeezing ($V_{\mathrm{SQ}}=0.1$). (d) Locus of unity gain points from no squeezing to perfect squeezing.

The amplitude squeezing of SQ3 enables, in theory, a perfect reproduction of the single amplitude quadrature fluctuation $\delta\hat{X}_V^+$. The complete polarization teleportation system now uses only an entangled pair and one additional squeezed beam.

An interesting characteristic of the measurement of the vertical polarization is that the signal transfer is best in the limit of infinite gain. On the other hand, the conditional variance of the vertical polarization cannot be improved as there are no correlations between the detected beam and the squeezed reconstruction beam.

It is possible, however, to represent the entire system on a single T-V diagram with $T_q=T_H^+ + T_H^- + T_V^+$ and $V_{\mathrm{cv}}=\frac{1}{3}(V_{\mathrm{cv,H}}^+ + V_{\mathrm{cv,H}}^- + V_{\mathrm{cv,V}}^+)$. Since the phase quadrature $\delta\hat{X}_V^-$ is irrelevant to the polarization description of the state [Eqs. (17)–(19)], it is reasonable not to include it in the T-V analysis, which relates to the polarization information transferred during the teleportation process.

For simplicity, the choice of $V_{\mathrm{SQ3}}=V_{\mathrm{SQ}}$ is made for the remainder of this section. Figure 6 shows a resulting three quadrature (X_H^+, X_H^-, X_V^+) T-V plot. For ideal squeezing of all three beams the minimum conditional variance $V_{\mathrm{cv}}\to 0$, and the maximum signal transfer coefficient $T_q\to 3$, can still be reached.

In the SQD scheme, beam SQ3 needs to be amplitude squeezed in order to reduce any noise in the signal quadrature. As a result, the phase quadrature becomes very noisy as $1/V_{\mathrm{SQ3}}\to\infty$. The unfavorable consequence of this is that the fidelity of the scheme is found to be vanishingly small. The fidelity equation (10) reduces to

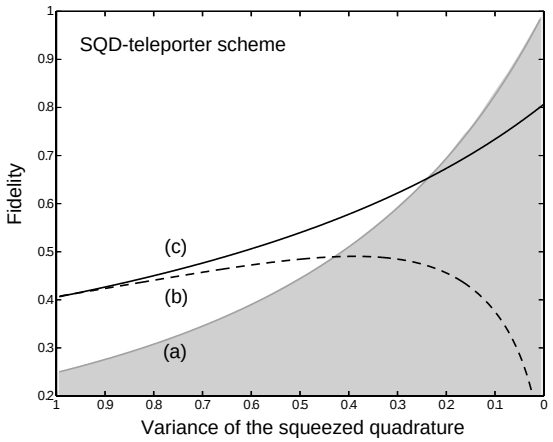

FIG. 7. The fidelity curves for (a) the twin teleporter system, (b) the SQD-teleporter system with $V_{SQ3}=V_{SQ}$, and (c) the SQD-teleporter system with no squeezing on the SQ3 beam.

$$\mathcal{F}_{SQD}=\frac{2}{(1+V_{SQ})\sqrt{(V_{SQ3}+2)\left(\frac{1}{V_{SQ3}}+1\right)}}. \qquad (20)$$

In fact, the maximum fidelity of the replicated quantum state is $\mathcal{F}=\sqrt{(2/3)}$, attained when there is no SQ3 squeezing at all and $V_{SQ}\rightarrow 0$. Figure 7 shows two possible fidelity curves, with and without SQ3 beam squeezing. The SQD-teleporter curve exceeds the results of the twin teleporters for all squeezing levels up to 80%, even though less resources are used. This is because there are fewer measurement penalties in the three beam case. When performing classical teleportation (i.e., teleportation with coherent states in place of entanglement) of all four quadratures, each quadrature reconstruction will degrade the fidelity. Classical teleportation of only three quadratures means the fourth quadrature is not degraded and therefore does not contribute to reducing the fidelity. The classical limit in the case of the SQD protocol may then be redefined by substituting $V_{SQ}=V_{SQ3}=1$ in Eq. (20), giving $\mathcal{F}=1/\sqrt{6}$.

VI. BIASED ENTANGLEMENT TELEPORTER SCHEME

It is somewhat disappointing that our SQD-teleporter scheme described in Sec. V performs worse in terms of fidelity when the SQ3 beam is squeezed [Figs. 7(b) and 7(c)]. In this section we present an alternative polarization teleportation scheme that also uses three squeezed beams but can perform better than the SQD-teleporter scheme in terms of fidelity.

Here, we use the third squeezed beam to generate entanglement of the vertical polarization. A single squeezed beam and a vacuum mode are combined on a beam splitter (labeled ε_1), the outputs of this beam splitter then exhibit *biased entanglement* [15]. That is, strong correlations are evident between the squeezed quadratures of the two outputs, but only shot-noise limited correlations exist between the beams for the orthogonal quadratures [15]. One of the biased entangled beams is then mixed with the vertical mode of the input state at the second beam splitter (labeled ε_2). The ability to choose the transmittivity of this beam splitter allows measurements of the amplitude quadrature of the vertical signal, which is equivalent to δS_1, or the phase quadrature of the vertical input, which is not represented on the Poincaré sphere, or to alternatively measure any combination of the two. The signal is then detected and fed forward to the modulators. We term this configuration biased entanglement teleportation (BET) (see Fig. 8).

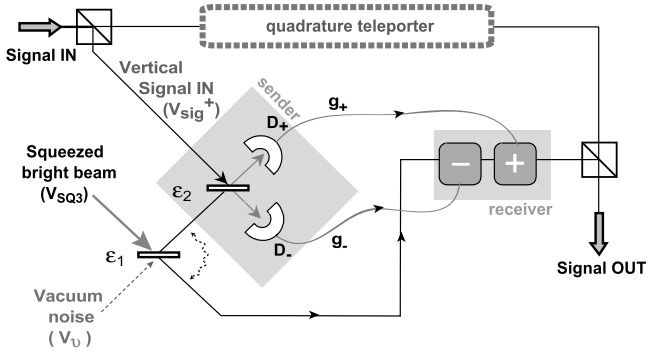

FIG. 8. Biased entanglement teleporter experimental setup. ε_1, the variable transmittivity beam splitter for biased entanglement of the inputs; ε_2, the variable transmittivity beam splitter for detection; $D_\pm$. amplitude/phase homodyne detection; $+/-$, amplitude/phase modulators; $g_\pm$, amplitude/phase feed-forward gains; and PBS, polarizing beam splitter.

The BET scheme can be thought of a modification of the twin teleporters, which tries to limit the resources from four bright, squeezed beams to only three. One EPR pair is still maximally entangled and teleports the horizontal fluctuations as before; however, the vertical information on the signal is teleported with one of the squeezed beams turned off. Further, the SQD-teleporter scheme from Sec. V is a special case of the BET scheme and can be recovered by setting $\varepsilon_1=1$ and $\varepsilon_2=0$.

The fidelity of a BET setup surpasses the $\mathcal{F}=\sqrt{(2/3)}$ direct detection limit. To do this, various parameters of the system can be optimized according to the value of squeezing injected, $V_{SQ3}^{\pm}$. The beam splitter transmittivities ε_1 and ε_2 can be changed to optimize Eq. (10). The amplitude modulator gain g_+ which relates to the vertically polarized signal quadrature needs to be kept at unity. The phase modulator gain g_-, however, relates to the quadrature with no information, and hence is optimized to minimize the reconstruction noise. Both gains are functions of ε_1, ε_2, and the squeezing $V_{SQ3}^{\pm}$. The polarity of g_+ and the quadrature being squeezed (either V_{SQ3}^{-} or V_{SQ3}^{+}), suggest four possible operating regimes. Our detailed analysis shows that three of these regimes have maximum fidelity surpassing that of the SQD-teleporter scheme. For the remainder of this section we will only discuss the best regime, which was obtained with feed-forward gain of $g_+>0$, and with the input phase squeezed ($V_{SQ3}^{-}<1$).

The improvement in the fidelity of the system occurs because at the extremes of squeezing ε_1 and $\varepsilon_2\rightarrow 0$, so that

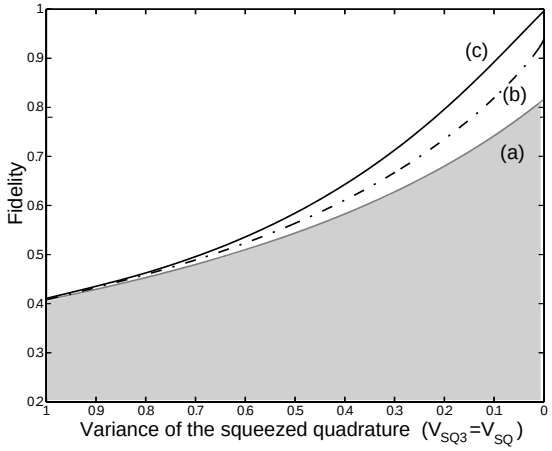

FIG. 9. The comparison of the fidelity curves for (a) the SQD-teleporter scheme, (b) the optimum BET scheme, and (c) the optimized twin teleporters. The schemes are all equivalent at low squeezing parameter.

almost all of the signal in the BET scheme is directed to the amplitude detector D_+ while most of the phase quadrature squeezing goes directly to the phase detector D_-. The modulation is then imprinted onto a nearly quantum noise limited beam. Some correlations exist between the detected phase fluctuations and the fluctuations of the output beam, which enable a cancellation of the output phase quadrature variance down to half the original shot noise level. The signal (amplitude) quadrature only pays the measurement penalty by coupling to a single unit of vacuum noise. For the biased entanglement part of the BET setup, pictured on the lower part of Fig. 8, the expression for fidelity in terms of the beam splitter ratios is given by

$$\mathcal{F}_{\max}=\frac{\mathcal{A}}{\sqrt{\mathcal{BC}}}, \tag{21}$$

where $\mathcal{A}$, $\mathcal{B}$, and $\mathcal{C}$ are given by

$$\mathcal{A}=2\sqrt{(\varepsilon_2-1)[\varepsilon_2(V^+_{\mathrm{SQ3}}-1)(\varepsilon_1-1)-\varepsilon_1(V^+_{\mathrm{SQ3}}-1)-1]}, \tag{22}$$

$$\mathcal{B}=2\varepsilon_2(V^+_{\mathrm{SQ3}}-1)(\varepsilon_1-1)-\varepsilon_1(V^+_{\mathrm{SQ3}}-1)-2, \tag{23}$$

$$\begin{aligned}\mathcal{C}=&\varepsilon_2[3-2\varepsilon_1+V^+_{\mathrm{SQ3}}(2\varepsilon_1-1)]\\&+2(V^+_{\mathrm{SQ3}}-1)\sqrt{\varepsilon_2(1-\varepsilon_2)\varepsilon_1(1-\varepsilon_1)}\\&-\varepsilon_1(V^+_{\mathrm{SQ3}}-1)-3,\end{aligned} \tag{24}$$

and we take $V^+_{\mathrm{SQ3}}=1/V^-_{\mathrm{SQ3}}$, with $V^-_{\mathrm{SQ3}}<1$.

Figure 9(b) shows a plot of the product of Eq. (21) and $\mathcal{F}=1/(V^+_{\mathrm{SQ}}+1)$, the fidelity of the quadrature teleporter with two equally amplitude squeezed beams ($V^+_{\mathrm{SQ}}<1$). It illustrates the fidelity of the optimum BET scheme by varying transmittivities ε_1 and ε_2 as a function of squeezing. The maximum reached at ideal squeezing is $\mathcal{F}=2\sqrt{2}/3\approx 0.943$. As expected, unity fidelity is never reached, however for all input squeezing levels the BET scheme is better than the SQD-teleporter scheme. Furthermore, the BET scheme can surpass the performance of the twin teleporters scheme introduced in Sec. IV at squeezing values within experimental reach. This scheme preserves the quantum nature of the complete state well but, as will be shown shortly, when information transfer is considered it is inferior to that of the SQD-teleporter scheme.

The evaluation of the transfer coefficient and conditional variance is also dependent on the optimization of gain, beam splitter ratios, and available squeezing parameters. However, the parameters optimized for fidelity do not necessarily correspond to the best T-V result. This occurs because fidelity weights every quadrature or Stokes operator equally, whereas T-V analysis concentrates on the information containing variables S_1, S_2, and S_3. The BET system then needs to be reoptimized and again, various regimes are reached depending on the transmittivities of ε_1 and ε_2. Our analysis shows that T^+_V and $V^+_{\mathrm{cv},V}$ as a function of feed-forward gain are optimized if the BET arrangement is set to recover the SQD-teleporter scheme of Fig. 6, by setting $\varepsilon_1=1$ and $\varepsilon_2=0$. Here the function $T^+_V=(4g^2_+)/(4g^2_++V^+_{\mathrm{SQ}})\rightarrow 1$, as $g_+\rightarrow\infty$. With greater squeezing, the transfer coefficient approaches unity more rapidly as g_+ increases. The amplitude quadrature conditional variance is independent of gain $V^+_{\mathrm{cv},V}=V^+_{\mathrm{SQ3}}$ and the minimum of zero occurs only in the limit of perfect squeezing.

It is clear from the above fidelity and T-V analysis that successful information transfer is not necessarily linked to an improvement in fidelity. When optimizing the fidelity, the BET protocol is weighted in favor of better state overlap. This means improving the output phase noise of the SQ3 beam. Reducing this phase noise, however, means sacrificing signal and reducing the signal transfer coefficient. The decision of which characterization method to use should be made dependening on the particular quantum information protocol for which the teleportation scheme is to be used.

VII. OPTIMIZED TWIN TELEPORTER SCHEME

The fidelity curve as a function of squeezing for the twin teleporters in Fig. 7(a) could also be optimized for the amplitude coded input signal considered in this paper. This can be achieved in a manner similar to the biased entanglement teleportation optimization, by adjusting the beam splitter transmittivities for each squeezing value. When all four inputs are equally squeezed ($V_{SQ3}=V_{SQ}=V_\nu$) and the pairs are 90° out of phase for best results, the fidelity is given by

$$\mathcal{F}_{4\mathrm{SQ}}=\frac{\mathcal{D}}{\sqrt{\mathcal{MN}}}, \tag{25}$$

where $\mathcal{D}$, $\mathcal{M}$, and $\mathcal{N}$ are given by

$$\mathcal{D}=2\sqrt{V_{\mathrm{SQ3}}^{+}(\varepsilon_2-1)[\varepsilon_2(V_{\mathrm{SQ3}}^{+}-1)[V_{\mathrm{SQ3}}^{+}(\varepsilon_1-1)+\varepsilon_1]+(V_{\mathrm{SQ3}}^{+})^2(1-\varepsilon_1)+\varepsilon_1]}, \tag{26}$$

$$\mathcal{M}=(1+V_{\mathrm{SQ3}}^{+})[\varepsilon_2(V_{\mathrm{SQ3}}^{+}-1)(1-2\varepsilon_1)+\varepsilon_1(V_{\mathrm{SQ3}}^{+}-1)-V_{\mathrm{SQ3}}^{+}],$$

$$\mathcal{N}=\varepsilon_2[1-2V_{\mathrm{SQ3}}^{+}-2\varepsilon_1-(V_{\mathrm{SQ3}}^{+})^2(1-2\varepsilon_1)]+[1-(V_{\mathrm{SQ3}}^{+})^2][\varepsilon_1-2\sqrt{\varepsilon_2(1-\varepsilon_2)\varepsilon_1(1-\varepsilon_1)}]+2V_{\mathrm{SQ3}}^{+}+(V_{\mathrm{SQ3}}^{+})^2. \tag{27}$$

Again, several regimes emerge; however, only the optimum regime for fidelity is considered here. This is shown in Fig. 9(c). The two optimized systems of BET [Fig. 9(b)] and twin teleporters show comparable results at lower values of the squeezing parameter, even though the twin teleporter requires more resources.

VIII. CONCLUSION

We have investigated schemes for the teleportation of polarization states carried by bright optical beams. We have shown that simply performing quadrature teleportation on the horizontal and vertical constituent modes separately is not optimal in terms of squeezing resources with respect to both the *T*-*V* and fidelity figures of merit. We introduce schemes that optimize the squeezing resources required for polarization teleportation with respect to each figure of merit. We find that the optimization is different depending on the figure of merit being used.

The difference in optimization of the two figures of merit can be understood in the following way. When small signals are applied to the polarization sidebands of a light field, they can be considered to be a two-mode coherent state $|\alpha_H\rangle|\alpha_V\rangle$. Due to our choice of basis, both figures of merit quantify the transfer of quantum information on the horizontal mode; however, they differ in how they treat the vertical mode. The *T*-*V* analysis considers the vertical mode to be a quantum limited classical channel. That is, it only considers the amplitude quadrature of the vertical mode, since the phase quadrature plays no role in determining the polarization of the composite field. On the other hand the fidelity analysis considers the vertical mode to carry quantum information on a restricted domain, with no classical signal present on its phase quadrature ($\delta X_{V,c}^{-}=0$). The appropriate figure of merit, and thus the most efficient teleportation protocol to use in a particular circumstance, depends on the way in which the quantum information is being encoded.

ACKNOWLEDGMENTS

This work was supported by the Australian Research Council and is part of the EU QIPC Project No. IST-1999-13071 (QUICOV). We are grateful to N. Treps and H.-A. Bachor for useful discussion.

[1] C.H. Bennett, G. Brassard, C. Crépeau, R. Jozsa, A. Peres, and W.K. Wootters, Phys. Rev. Lett. **70**, 1895 (1993).
[2] D. Bouwmeester, J.-W. Pan, K. Mattle, M. Eibl, H. Weinfurter, and A. Zeilinger, Nature (London) **390**, 575 (1997).
[3] A. Furusawa, J.L. Sørensen, S.L. Braunstein, C.A. Fuchs, H.J. Kimble, and E.S. Polzik, Science **282**, 706 (1998).
[4] W.P. Bowen, N. Trepps, B.C. Buchler, R. Schnabel, T.C. Ralph, H.-A. Bachor, T. Symul, and P.K. Lam, Phys. Rev. A **67**, 032302 (2002).
[5] J. Heersink, T. Gaber, S. Lorenz, O. Glöckl, N. Korolkova, and G. Leuchs, Phys. Rev. A **68**, 013815 (2003).
[6] V. Josse, A. Dantan, A. Bramati, M. Pinard, and E. Giacobino, J. Opt. B: Quantum Semiclassical Opt. **5**, S513 (2003).
[7] P. Grangier, R.E. Slusher, B. Yurke, and A. LaPorta, Phys. Rev. Lett. **59**, 2153 (1987).
[8] J. Hald, J.L. Sørensen, C. Schori, and E.S. Polzik, Phys. Rev. Lett. **83**, 1319 (1999).
[9] W.P. Bowen, R. Schnabel, H.-A. Bachor, and P.K. Lam, Phys. Rev. Lett. **88**, 093601 (2002); R. Schnabel, W.P. Bowen, N. Treps, T.C. Ralph, H.-A. Bachor, and P.K. Lam, Phys. Rev. A **67**, 012316 (2003).
[10] W.P. Bowen, N. Treps, R. Schnabel, and P.K. Lam, Phys. Rev. Lett. **89**, 253601 (2002).
[11] N. Korolkova, G. Leuchs, R. Loudon, T.C. Ralph, and Ch. Silberhorn, Phys. Rev. A **65**, 052306 (2002).
[12] G.G. Stokes, Trans. Cambridge Philos. Soc. **9**, 399 (1852); H. Poincaré, *Théorie Mathematique de la Lumière* (Corré, Paris, 1892), Vol. 2.
[13] B. A. Robson, *The Theory of Polarization Phenomena* (Oxford New York, 1974).
[14] J. M. Jauch and F. Rohrlich, *The Theory of Photons and Electrons*, 2nd ed. (Springer, New York, 1976).
[15] W.P. Bowen, P.K. Lam, and T.C. Ralph, J. Mod. Opt. **50**, 801 (2003).
[16] T.C. Ralph and P.K. Lam, Phys. Rev. Lett. **81**, 5668 (1998).
[17] F. Grosshans and P. Grangier, Phys. Rev. A **64**, 010301(R) (2001); P. Grangier and F. Grosshans, e-print quant-ph/0009079.
[18] R.E.S. Polkinghorne and T.C. Ralph, Phys. Rev. Lett. **83**, 2095 (1999).
[19] R. Bruckmeier, H. Hansen, S. Schiller, and J. Mlynek, Phys. Rev. Lett. **79**, 43 (1997).